Proceedings of the 20th International Conference on Soil Mechanics and Geotechnical Engineering– Rahman and Jaksa (Eds)

Conceptual physical modelling of a subsurface geomembrane energy storage system

Modélisation physique conceptuelle d'un système de stockage d'énergie geomembrane souterrain

Kenny Kataoka Sørensen, Hans Henning Stutz, Phivos Brødsgaard-Raptis & Martin Luxhøj
Department of Civil and Architectural Engineering, Aarhus University, Denmark, kks@cae.au.dk

ABSTRACT: This paper focuses on physical modelling of a novel Underground Pumped Hydro-electric Storage (UPHS) system for storing energy. Potential energy is stored by pumping water into a shallow buried reservoir enclosed by a water-tight flexible geomembrane. An updated reservoir geometry design is used to overcome previously seen issues with overstressing of the membrane and at the same time to increase the storage capacity per unit area. A 2.5m diameter small-scale (1:100) 1g physical model of the system was created using sand as overburden, and the laboratory test setup was used to demonstrate the conceptual behaviour and to investigate energy loss characteristics of the system under repeated inflation-deflation cycles of the membrane reservoir. In addition, interface testing has been carried out to investigate the interface shearing behavior between two different membrane types and sand to further understand the interface shearing mechanisms and membrane wear occurring at full scale pressures. The physical small-scale and lab tests will help to identify areas which need further attention.

RÉSUMÉ : Cet article met l'accent sur la modélisation physique d'un nouveau système souterrain de stockage hydro-électrique pompé (UPHS) pour stocker l'énergie. L'énergie potentielle est stockée en pompant l'eau dans un réservoir enfoui peu profond entouré d'une géomembrane flexible étanche à l'eau. Une conception mise à jour de la géométrie du réservoir est utilisée pour surmonter les problèmes précédemment observés avec le surentrage de la membrane et en même temps pour augmenter la capacité de stockage par unité de surface. Un modèle physique à petite échelle de 2,5 m de diamètre (1:100) 1 g du système a été créé en utilisant le sable comme surcharge, et la configuration des essais en laboratoire a été utilisée pour démontrer le comportement conceptuel et étudier les caractéristiques de perte d'énergie du système dans le cadre des cycles répétés inflation-déflation du réservoir membranaire. En outre, des tests d'interface ont été effectués pour étudier le comportement de cisaillement de l'interface entre deux types de membranes différents et le sable afin de mieux comprendre les mécanismes de cisaillement de l'interface et l'usure de la membrane qui se produisent à pleine échelle. Les tests physiques à petite échelle et en laboratoire aideront à identifier les domaines qui ont besoin d'une attention accrue.

KEYWORDS: geomembrane, energy storage, interface shearing behavior, physical model testing

1 INTRODUCTION

The increasing use of renewable sources of energy necessitates an increasing focus on finding suitable solutions for storing excess energy (Barnes and Levine, 2011). This paper focuses on physical modelling of a new concept system for storing energy. The concept is a modified version of the Pumped Hydroelectric Energy Storage (PHES) system. However, instead of pumping water up to great height, water is pumped into a shallow buried reservoir enclosed by a water-tight flexible geomembrane, as illustrated in Figure 1.

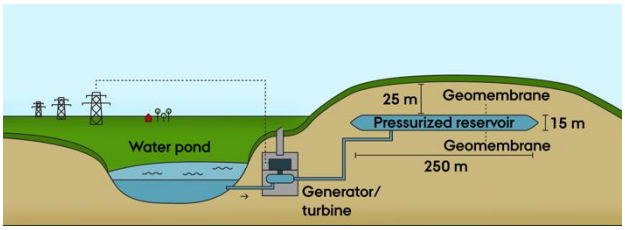

Figure 1. Illustration of underground pumped hydro storage (UPHS) concept

Potential energy is stored by inflation and pressurisation of the reservoir with water and lifting of the overlying mass of soil. A turbine/generator is used to convert the stored energy to electricity when the water is returned to a nearby pond or reservoir. The general principle of the so-called Underground Pumped Hydro-electric Storage (UPHS) system was presented by Olsen et al. (2015).

Further development of the system has continued and to overcome previously seen issues with overstressing of the membrane and to increase storage capacity an updated reservoir geometry design is considered in this study. The system is updated considering a circular geometry with a cavity shaped as a bowl with upwards sloping perimeter (illustrated in Figure 1) which allows for a greater lift height and hence an increase in stored potential energy.

A finite-element model of the energy storage system has been developed and presented by Norlyk et al. (2020) and Stutz et al. (2020) who demonstrate that the model is able to capture and simulate realistic system behaviour under cyclic inflation and deflation of the reservoir.

If the hydrodynamic losses in the system is not considered the stored energy $E_{storage}$ [J] of a circular reservoir with diameter D [m], a total lift height H_t [m] and height of overburden H_s [m] can be estimated by:

$$E_{storage} = \int_0^V p\, dV = \frac{\pi}{4} D^2 H_t (\gamma_s H_s + 0.5 \gamma_w H_t) \quad (1)$$

where γ_s and γ_w is the unit weight of the overburden soil and water respectively [N/m^3]. Hence for the illustrated large-scale pilot plant with a diameter of 250 m, a lift height of 15 m and thickness of overburden soil of 25 m, the stored capacity will be approximately 107 MWh assuming the overburden soil has a unit weight of 18 kN/m^3.

In this preliminary study the interaction between soil-membrane-water under the action of repeated inflation and deflation of the water reservoir is studied. 1g physical model testing at reduced scale (1:100) have been carried out in the laboratory to validate the concept, to investigate the overall system behaviour and to illustrate variations in energy loss from internal shearing and creep in the overburden sand. In addition, interface shear testing has been performed to investigate the wear of the membrane and shear behaviour of the soil-membrane interface under repeated cyclic loading at full scale pressures. This paper presents some of the preliminary results.

1.1 *Materials and methods*

1.1.1 *Characterisation of overburden sand and geomembranes*

A uniform sand with semi rounded grains (Dansand Superdress) with particle sizes ranging between 0.125 and 1 mm was used in this study as overburden soil in the physical model test and in the performed interface tests. The characteristic physical properties of the sand are shown in Table 1.

Figure 2a shows a photo of the soil grains. The roundness defined as the ratio of the average radius of curvature of the corners of a particle to the radius of the maximum inscribed circle was determined using computational geometry as described by Zheng & Hryciw (2015) and illustrated in Figure 2b.

Table 1. Characterisation of overburden sand (Dansand Superdress) used in physical model test and interface shear test

Specific gravity of soil G_s	2.69
Mean grain size d_{50} (mm)	0.355
Coefficient of uniformity d_{60}/d_{10}	1.9
Roundness of grains	0.73
Min./Max. void ratio[1]	0.56/0.87
Angle of shearing resistance $\varphi'_{peak}/\varphi'_{cs}$ (°)[2]	38/35

[1] Laboratory fall weight tampering according to DGF (2001)
[2] Direct shear tests at a normal stress level of 190-560 kPa and average void ratio of 0.62 at critical state

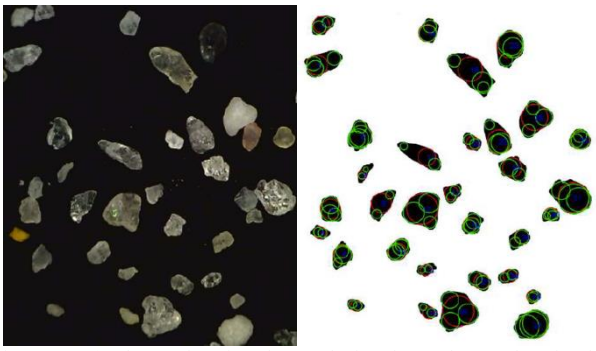

Figure 2. (a) Photo of grains (b) Analysis of roundness of grains by computational geometry

For the full-scale geomembrane energy storage system, a number of suitable geomembranes are being considered. The properties of the upper geomembrane are especially relevant, as it will be subjected to cyclic loading, undergo folding and to some degree stretching as the water reservoir is filled and emptied. In addition, the geomembrane will be buried and in direct contact with the overburden soil and experience seasonal changes in humidity and temperature at the interface to the overburden soil. Hence, a flexible and durable smooth geomembrane with high tensile strength and high yield strain is desirable. Two geomembranes manufactured by Solmax GSE have been considered relevant to test in this study;

A. GSE Proflex - which is a smooth Propylene/ethylene copolymer (EPM).
B. GSE Ultraflex - which is smooth Linear Low Density PolyEthylene (LLDPE)

Both membranes are produced in various thicknesses, but the standard thickness is typically 2mm which is flexible enough to handle, yet strong and stiff enough to be suitable for application in the proposed full-scale system. Wear of both geomembranes have been tested in interface shear tests in this study.

For the small-scale physical model test a membrane replacement with a lower rigidity had to be chosen to avoid significant scaling effects due to variation in the membrane to sand rigidity ratio. For practical reasons it is not possible to scale the membrane thickness to 1:100. A standard transparent 0.2 mm LDPE foil was chosen to represent the geomembranes in the small-scale physical model test. Although the foil is only 1/10th of the full-scale thickness and its tensile stiffness is approximately 4 times greater than EPM, it is expected that the soil to membrane rigidity ratio is sufficiently small to allow for realistic system behaviour.

The properties of the tested membranes are listed in Table 2.

Table 2. Characterisation of geomembranes used in interface shear test (type A and B) and physical model test (type C)

	A *GSE Proflex*	*B* *GSE Ultraflex*	*C* *Foil*
Material	EPM	LLDPE	LDPE
Thickness (mm)	2.0	1.0	0.2
Density (g/cm^3)	0.89	0.94	0.92
Young's modulus (MPa)	90		335 [2]
Stress at break (MPa)	19 [1]	33 [1]	462 [2]
Elongation at break (%)	900 [1]	900 [1]	630 [2]

[1] DIN EN ISO 527-3 TYPE 5; 100 mm/min 50 mm gauge length
[2] Average values from https://polymerdatabase.com

1.1.2 *Cyclic interface shearing testing*

Interface testing was carried out in a modified Direct shear device (Stutz et al. 2018) in which the lower part of the shear box has been replaced with a geomembrane surface (Figure 3). Similar test devices have been used by Martinez & Stutz (2018) for soil-structure interface research. The stress conditions and sample preparation were identical to the Direct Shear tests. The shear box has a size of 100mm x 63.5 mm x 32.5 mm. The tests were conducted as half-cycle tests with 10 mm displacement and 1 mm/min displacement rate.

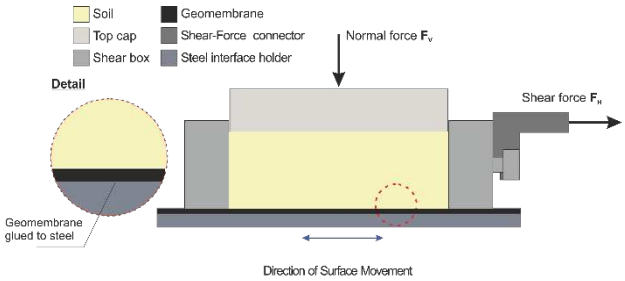

Figure 3. Illustration of Interface shear test device with test arrangement

The interface tests were carried out with the two different membranes. A maximum of 50 cycles per test were performed. The surfaces were scanned before and after each test at varying number of cycles to estimate the evolution of wear and improve the understanding of the wear behaviour of the geomembrane under the real in-situ pressures. The membrane material was glued to a steel surface to prevent wrinkling of the membrane material under the cyclic test.

1.1.3 *Measurement of surface rougness of geomembranes*

The wear of the membrane surface during cyclic shearing was quantified by the change in surface roughness. A one-shot Measuring Macroscope VR-3000 from Keyence was used in accordance with ISO4287:1997 to obtain a measure of the surface roughness in a central area of 25x50 mm on the membrane. The average roughness R_{max} was determined along two cross sections within this area; one in the direction of shearing and one in the orthogonal direction. R_{max} is defined as the distance from the bottom of the lowest point to the top of the highest within a reference length of 0.3 mm, roughly equal to d_{50} of the sand.

1.1.4 *Lg small-scale physical model testing*

A small-scale physical 1g model setup was constructed in the lab at roughly 1:100 scale. Although the thickness of the overburden was slightly increased, then it is clear that realistic full scale in-situ stresses in the soil cannot be achieved. Hence, this will have a significant impact on the internal shearing of the sand. Despite the incorrect scaling of the overburden pressures, then it is believed that the simple (1g) physical model can be used to support the validation of the concept by illustrating the overall system behaviour. The shape of the model was chosen to be cylindrical to allow for validation of and comparison with an axisymmetric numerical model (Norlyk et al. 2020). The geomembrane reservoir was 2.5 m in diameter with 0.5 m air-dried loose overburden sand on top.

A closed loop automatic pumping system was made using electro valves and a Grundfos pump (CME1-2 A-R-I-E-AQQE) to control the flow of water in and out of the reservoir. 22 mm diameter stainless steel pipes were used in the system, and flow was monitored using a vortex flow sensor (F) and water pressure was monitored using a Danfoss pressure gauge (MBS 33) placed just outside the reservoir (P) on the central flow line. A nominal flow rate of 0.4 m^3/hr ~ 6.7 L/min was used, but the flow rate was observed to gradually reduce during inflation from roughly 6.7 to 6.1 L/min and from 7.3 to 6.7 L/min during deflation (see Figure 7).

In fully inflated position, the upper membrane and overburden sand are lifted on average 0.15 m above the lower membrane and in this position the reservoir holds 0.625 m^3 of pressurised water in storage corresponding to 2 Wh capacity. The small-scale physical model setup is illustrated in Figure 4.

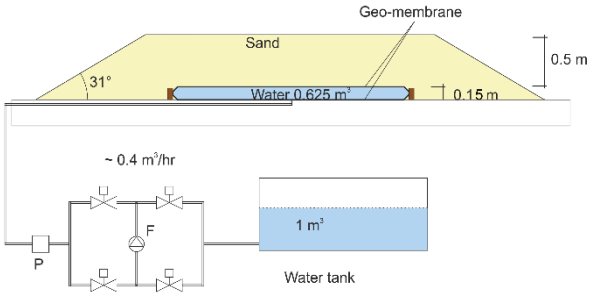

Figure 4. Illustration of physical 1:100 scale model of an UPHS system with fully inflated water reservoir.

This paper reports the results from two tests performed with and without overburden sand with the setup shown in Figure 4. Ten cycles of inflation and deflation were carried out to study the evolution of energy loss in the overburden sand over a period of 32 hours.

Additional tests have been carried out with different overburden geometries and design of the membrane reservoir (Brødsgaard-Raptis & Luxhøj, 2019), but it has been out of the scope of this paper to present these results.

2 OBSERVED BEHAVIOUR DURING INFLATION AND DEFLATION OF THE SMALL-SCALE GEOMEMBRANE RESERVOIR

2.1 *Pressure variation*

The inflation and deflation of the reservoir without overburden sand serves as a reference for the subsequent inflation and deflation of the reservoir with overburden sand. In Figure 5 the variation of water pressure is plotted against stored volume of water in the reservoir as the reservoir is inflated and subsequently deflated for the first time. Series of data are shown for the case with and without overburden sand respectively and best fit linear trendlines for inflation and deflation are shown on the plot. The absolute pressures have been zero shifted by the same amount to ensure an initial measured pressure of zero at the start of inflation of the reservoir without overburden sand. The initial pressure (= 8kPa) with 0.5 m overburden sand corresponds to a credible unit weight of the sand of 16 kN/m^3 which is equivalent to a void ratio of 0.68 and a relative density of 61%.

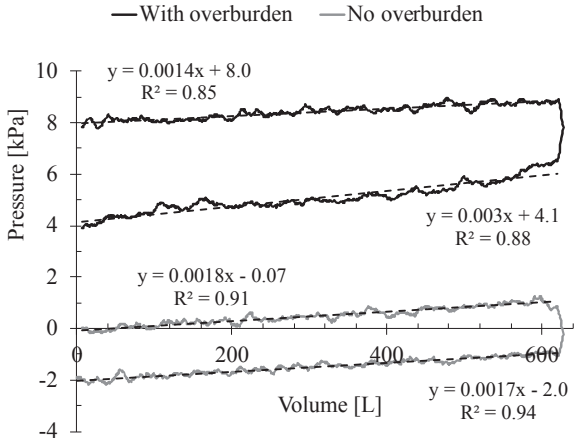

Figure 5. Variation of water pressure during inflation and deflation of the water reservoir – without overburden sand

The pressure in the reservoir is seen to increase steadily with increasing inflation as expected. Without any overburden and assuming simple hydrostatic pressure conditions the expected increase in pressure during inflation to a lift height of approximately 0.15 m will be 1.5 kPa. This corresponds to 0.0024 kPa/L of water pumped into the reservoir. As can be seen from the slope of the best fit linear trendline shown on Figure 5 the observed response during inflation with no overburden is slightly lower and on average 0.0018 kPa/L. Whilst the pressure increase is seen to drop to around 0.0014 kPa/L during inflation of the reservoir with overburden. This highlights that the pressure from the overburden alone reduces during the first inflation as a result of reduction in overburden height due to instability of the sand surface at the edge zones. The difference corresponds to a loss of around 1.4 cm in overburden height during the first inflation if internal stresses in the sand are ignored.

A rapid drop and increase in the pressure are observed in Figure 5 as a response to a reversal of the flow direction at full inflation and deflation respectively for both situations with and without overburden sand. This can be seen as a change in the dynamic pressure acting on the pressure gauge which is observed to result in almost perfectly linear relations between pressure and volume changes until a more stable flow condition is established again. A dynamic pressure drop of 2 kPa is found with no overburden, while the pressure drop is found to be 2.9 kPa with overburden.

It would generally have been more appropriate to place the pressure sensor on a separate access line away from the main flow inlet to minimize the influence of the dynamic pressure.

Nevertheless, if the pressure response is corrected for the dynamic pressure then the pressure – volume response with no overburden is seen to be fully reversible with no loss of energy as shown on Figure 6. Whereas the corrected pressure response in the setup with overburden sand clearly indicate hysteresis resulting from energy dissipation due to internal shearing, creep and redistribution of stresses within the overburden sand.

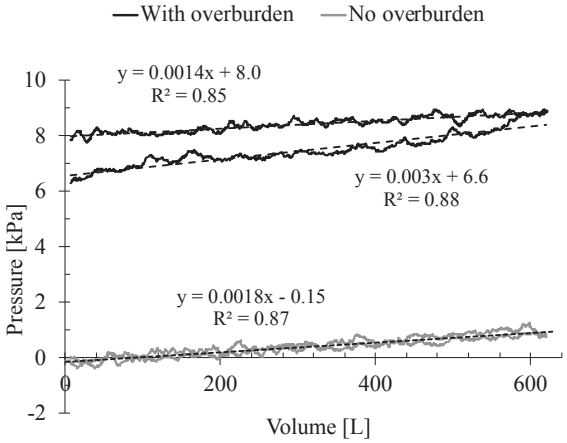

Figure 6. Corrected variation of water pressure during 1st cycle of inflation and deflation of the water reservoir – with and without overburden sand

10 cycles of inflation and deflation were performed to investigate the system response with overburden sand during cyclic loading. The variation in pressure and flow during the duration of the test is shown in Figure 7, while the associated pressure-volume response is seen from Figure 8.

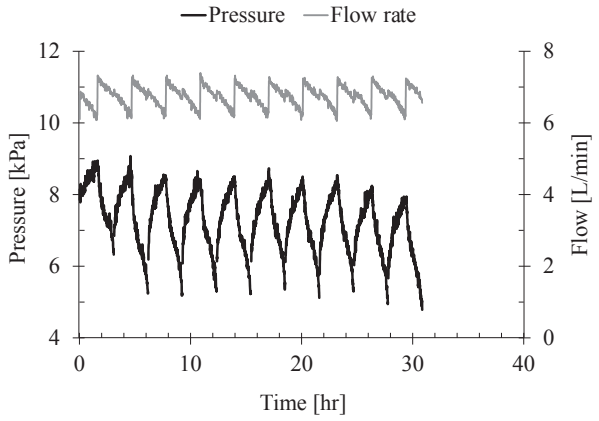

Figure 7. Variation of corrected water pressure and flow during 10 cycles of inflation and deflation of the water reservoir – with overburden sand

The variation in pressure indicate that the aforementioned instability at the edges of the overburden is mainly an issue during the first couple of cycles. After the third cycle the pressure-volume response shows only little change although a further reduction is seen in the last two cycles. Observations made during testing support that shallow surface slips occur at the edge zones primarily during the initial cycles.

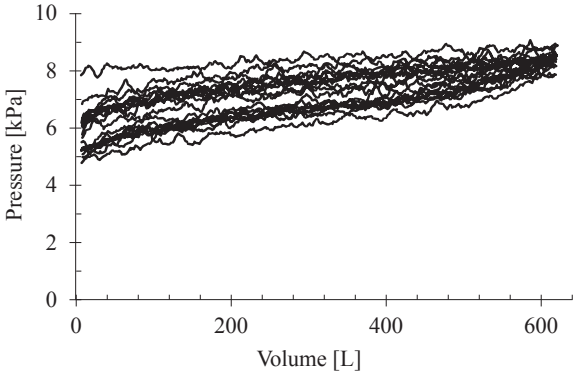

Figure 8. Variation of corrected water pressure during 10 cycles of inflation and deflation of the water reservoir – with overburden sand

2.2 *Energy loss*

The added and returned energy E [J] during inflation and deflation of the reservoir can be calculated based on the measured variation of pressure p [kPa] and the change in volume V [L] as given by equation 1. Hence the energy loss E_{loss} arising due to internal shearing and creep in the overburden sand can be determined from the difference in added and returned energy:

$$E_{loss} = \int_{V_0}^{V_1} p\, dV - \int_{V_1}^{V_0} p\, dV \quad (2)$$

The evolution in the added and returned energy during inflation and deflation respectively from 1 to 10 cycles is shown in Figure 9 alongside the variation in the energy loss given as a percentage of the added energy. As was also indicated from Figure 7, it can be seen that the added and returned energy initially reduce during the first two cycles and subsequently remains almost constant until the last cycle. After the first 3 cycles the energy loss is found to be reasonably constant with an average of approximately 11%.

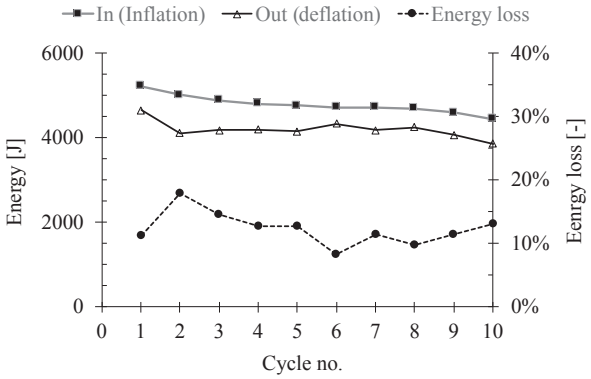

Figure 9. Evolution in added and returned energy, and energy loss with increasing cycles of inflation and deflation

The average energy loss in the overburden sand (~2.5 m^3) over the last 6 cycles is 215 J/m^3. If it is assumed that the energy loss per volume of overburden sand remains constant as the system is scaled up, then this leads to an estimated energy loss in the overburden sand of less than 0.1 % of the storage capacity in a 250 m diameter large-scale pilot plant. However, the incorrect scaling of the stresses in the 1g physical model test means that this assumption is likely to be invalid, and the determined energy loss per volume of sand (or in % of added energy) is likely to overestimate the energy loss at greater pressure due to significant non-linear stress-strain behaviour and plastic straining of sand at small stresses.

Nevertheless, as the system is scaled up the energy loss contribution from the overburden sand can be expected to

become insignificant, as found by Olsen et al. (2015), and the majority of energy loss will occur due to friction in the piping and pumping system.

3 OBSERVED CYCLIC INTERFACE SHEARING BEHAVIOUR BETWEEN SAND AND GEOMEMBRANE

3.1 *Cyclic interface shearing behaviour*

The cyclic interface geomembrane-soil tests were conducted with the two different geomembranes. As indicated by Zettler et al. (2000), it can be expected that for stress higher than 75 kPa at the soil-geomembrane shear-induced irreversible changes will occur. This is primarily due to ploughing of the granular material into the geomembrane and can mainly be influenced by the hardness of the membrane material (Dove and Frost, 1999).

To estimate the soil-geomembrane behaviour, four shear tests with respectively 2 , 10, 30 and 50 cycles have been performed with each of the two investigated membrane materials. The shear stress –displacement response is shown in Figure 10 for the Ultraflex (a) and Proflex (b) membrane. The shear stress displacement response for the Ultraflex can be considered constant during the different cycles. Whereas the GSE Proflex show initial lower shear stress with an initial increase until the 30th cycle.

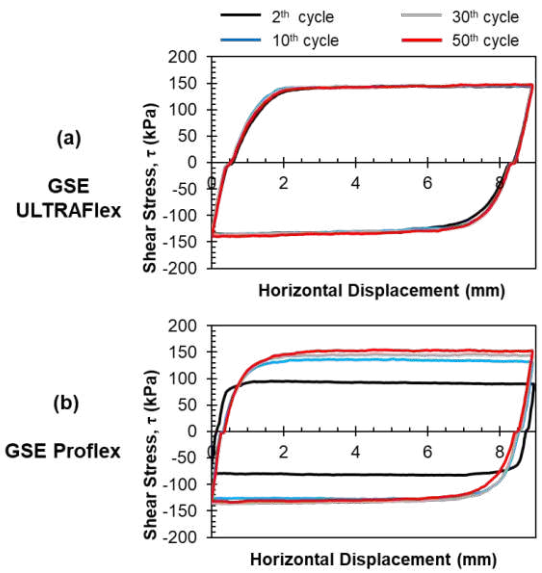

Figure 10. Shear stress vs shear displacement at σ_n = 250 kPa for the different number of cycles. GSE ultraflex results are shown in (a). GSE Proflex results are shown in (b)

The two different membrane behaviours are attributed to the different stiffness of the membrane material (see Table 2). The angle of friction at the interface is around 26 ° compared to 35° for sand. The reason for this difference is the smooth geomembrane surface. Consequently, sliding and rolling of the grains at the interface surface is the primary deformation mode as compared to more complex grain interactions in the direct shear test.

3.2 *Membrane wear during cyclic shearing*

Upon completion of the cyclic interface testing the ploughing induced wear damage of the membrane was measured after the different cycles (Figure 11 and 12). Whereas the Ultraflex membrane shows an increase in roughness, followed by a decrease for a higher number of cycles (Figure 11), the Proflex membrane showed only an increase in roughness. The change in roughness is attributed to wear damage of the membrane due to the granular material.

Both membrane materials show increasing wear due to higher effective stress, as mentioned by Dove & Frost (1999). In contrast, to Dove & Frost (1999), the increase of the wear is not a linear relationship, as shown in Figures 11 and 12. Dependent on the membrane material after an increase until the 25th cycle, the membrane roughness decrease for the Proflex material under cyclic shearing. Both membrane materials (Figure 11 & 12) show smaller incremental damage with increasing effective stresses.

It is observed from the shear stress evolution and the wear damage for the Proflex material that the changes in the membrane roughness lead to a change of the shear stresses (Figure 10b, and 12). A similar link is however not observed for the stiffer Ultraflex material. Considering the membranes' different mechanical properties, it is assumed that these properties are most influential for the observed behaviour. A more extensive study considering the micromechanical grain-membrane interaction is needed to clarify this.

Besides the test results mentioned above for the application of the UPHS system in real scale, it will be essential to consider the manufacturing process of the geomembrane and the induced surface roughness changes (Frost et al. 2002).

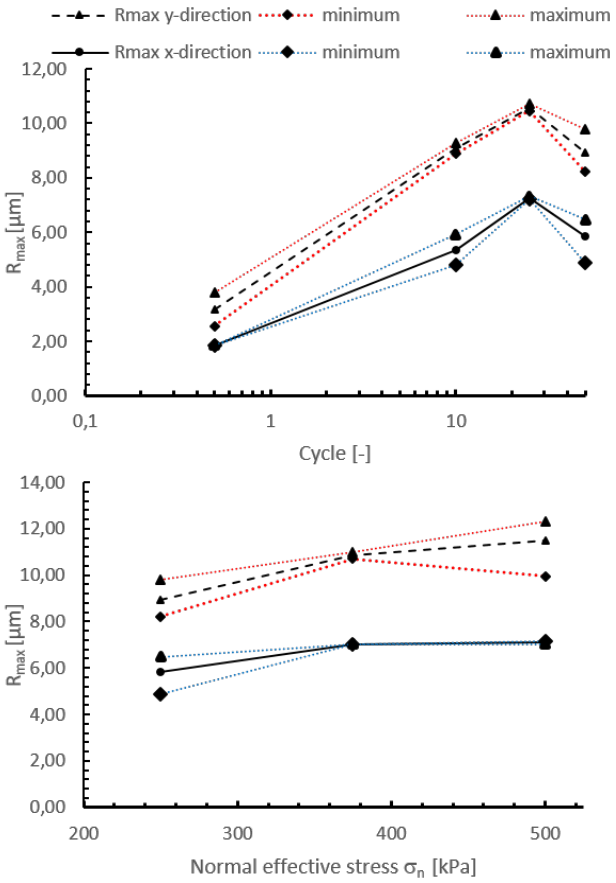

Figure 11. R_{max} versus number of cycles at σ_n = 250 kPa, and R_{max} versus normal effective stress after 50 cycles, in the shear direction (x) and across the shear direction (y) for the GSE Ultraflex membrane

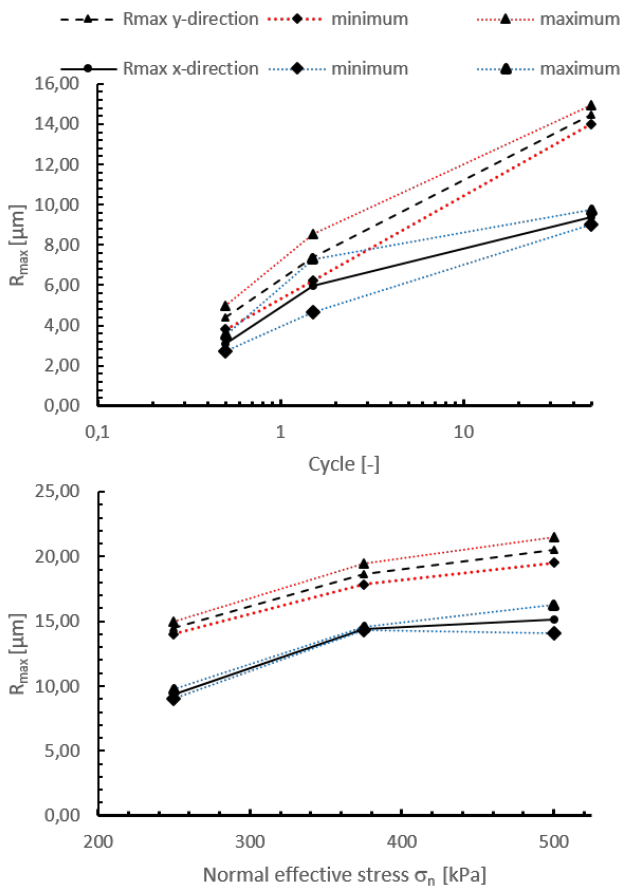

Figure 12 R_{max} versus number of cycles at σ_n = 250 kPa, and R_{max} versus normal effective stress after 50 cycles, in the shear direction (x) and across the shear direction (y) for the GSE Proflex membrane

4 CONCLUSIONS

The performed 1g physical small-scale model test demonstrated the conceptual behaviour of the UPHS system for storing energy. Observed hysteresis in the pressure-flow measurements during inflation and deflation arises from internal shearing and creep in the overburden sand which leads to energy losses in the system. The energy loss is furthermore found to be influenced by instability of the edge zones in the overburden during the first cycles of inflation and deflation after which it stabilises at around 11%. The energy loss is found to be relativity high due to the small-scale and low pressures employed in the model. Further testing at larger scale and physical model testing at elevated pressure is needed to validate the system behaviour and to obtain a better estimate of the expected energy loss within the overburden sand.

The performed interface shearing tests have shown the damage of the membrane considering the cyclic loading during inflation and deflation. Generally, the membrane wear is found to increase with increasing stress level, however interestingly, an increase in roughness is seen followed by a decrease in roughness with increasing cycles for the Proflex membrane at a normal stress of 250 kPa, whereas the Ultraflex shows only an increase in R_{max}. In the main parts of the full-scale UPHS system the stresses will be greater than 250 kPa. The conducted study highlights the need for a larger cyclic testing campaign under the planned in-situ stress considering the interface wear and damage behaviour.

5 ACKNOWLEDGEMENT

This research was supported by Innovation Fund Denmark via the InnoSE and Innobooster funding schemes. The financial support is much appreciated. Furthermore, the authors wish to thank Asger Gramkow and Hans Christian Fejborg from AquaNamic for providing insight and expertise that greatly assisted the research. However, all results presented in this paper are under the full responsibility of the authors and do not necessarily reflect the opinions of the persons mentioned above.

6 REFERENCES

Barnes, F.S., Levine, J.G., 2011. Large Energy Storage Systems Handbook. CRC Press.

Brødsgaard-Raptis P. M. & Luxhøj M. N. 2019. Underground pumped hydro-electrical storage. Department of Engineering, Aarhus University, Internal report.

DGF 2001. Relativ lejringstæthed. Laboratoriehåndbogen. dgf-Bulletin 15.

Dove J.E. & Frost, J.D. 1999. Peak friction behaviour of smooth geomembrane-particle interfaces, Journal of Geotechnical and Geoenviromental Engineering, Vol 125, No. 7, pp. 544-555

Frost, J.D., Zettler, T.E., DeJong, J.T., Lee, S.W., Kagbo, S. (2002) Strain induced changes in geomembrane surface topography, Geosynthetics International, Vol. 9 No. 1, pp. 21-39

Fuggle, A.R. & Frost, J.D. 2010. Particle size effects on interface shear behaviour and geomembrane wear, in Charaterisation and Behaviour of Interfaces, J.D. Frost, (Ed.), IOS Press, pp. 51-57

Martinez, A & Stutz, H.H. 2019. 'Rate effects on the interface shear behaviour of normally and over-consolidated clay', Geotechnique, vol. 69, no. 9, pp. 801-815. https://doi.org/10.1680/jgeot.17.P.311

Norlyk P., Sørensen K., Andersen L.V., Sørensen K.K. & Stutz H.H. 2020. Holistic simulation of a subsurface inflatable geotechnical energy storage system using fluid cavity elements. Computers and Geotechnics, Volume **127**, 103722, https://doi.org/10.1016/j.compgeo.2020.103722.

Olsen J., Paasch K., Lassen B., Veje C. T. 2015. A new principle for under-ground pumped hydroelectric storage. Journal of Energy Storage 2, pp. 54–63.

Patent DK179739B1 – System for Storage of Energy and/or Water.

Stutz, H. , Doose, R.& Wuttke F. 2018. "Open Science Interface Shear Device". in Wu, W. Yu, H.S. (editors). Proceedings of China-Europe Conference on Geotechnical Engineering. Springer. (Springer Series in Geomechanics and Geoengineering , Vol. 1). pp. 615-618.

Stutz H.H., Norlyk P., Sørensen K., Andersen L.V., Sørensen K.K. & Clausen J. 2020. Finite element modelling of an energy-membrane underground pumped hydroelectric energy storage system. 2nd International Conference on Energy Geotechnics, La Jolla, California, USA. E3S Web Conf., 205 (2020) 07001 https://doi.org/10.1051/e3sconf/202020507001

Zheng J. and Hryciw R.D. 2015. Traditional soil particle sphericity, roundness and surface roughness by computational geometry. Géotechnique, 65(6), pp. 494-506.